J. Fluid Mech. (2008), *vol.* 602, *pp.* 287–302.
doi:10.1017/S0022112008000992 Printed in the United Kingdom

On the deficiency of even-order structure functions as inertial-range diagnostics

P. A. DAVIDSON[1] AND P.-Å. KROGSTAD[2]

[1]Department of Engineering, University of Cambridge, Cambridge CB2 1PZ, UK
[2]Department of Energy and Process Engineering, Norwegian University of Science and Technology, N-7491 Trondheim, Norway

(Received 16 February 2007 and in revised form 29 January 2008)

In the limit of vanishing viscosity, $\nu \to 0$, Kolmogorov's two-thirds, $\langle(\Delta v)^2\rangle \sim \epsilon^{2/3} r^{2/3}$, and five-thirds, $E \sim \epsilon^{2/3} k^{-5/3}$, laws are formally equivalent. (Here $\langle(\Delta v)^2\rangle$ is the second-order structure function, ϵ the dissipation rate, r the separation in physical space, E the three-dimensional energy spectrum, and k the wavenumber.) However, for the Reynolds numbers encountered in terrestrial experiments, or numerical simulations, it is invariably easier to observe the five-thirds law. We ask why this should be. To this end, we create artificial fields of isotropic turbulence composed of a random sea of Gaussian eddies whose size and energy distribution can be controlled. We choose the energy of eddies of scale, s, to vary as $s^{2/3}$, in accordance with Kolmogorov's 1941 law, and vary the range of scales, $\gamma = s_{\max}/s_{\min}$, in any one realization from $\gamma = 25$ to $\gamma = 800$. This is equivalent to varying the Reynolds number in an experiment from $R_\lambda = 60$ to $R_\lambda = 600$. We find that, while there is some evidence of a five-thirds law for $\gamma > 50$ ($R_\lambda > 100$), the two-thirds law only starts to become apparent when γ approaches 200 ($R_\lambda \sim 240$). The reason for this discrepancy is that the second-order structure function is a poor filter, mixing information about energy and enstrophy, and from scales larger and smaller than r. In particular, in the inertial range, $\langle(\Delta v)^2\rangle$ takes the form of a mixed power law, $a_1 + a_2 r^2 + a_3 r^{2/3}$, where $a_2 r^2$ tracks the variation in enstrophy and $a_3 r^{2/3}$ the variation in energy. These findings are shown to be consistent with experimental data where the 'pollution' of the $r^{2/3}$ law by the enstrophy contribution, $a_2 r^2$, is clearly evident. We show that higher-order structure functions (of even order) suffer from a similar deficiency.

1. Introduction

There are three diagnostic tools commonly used to give an impression of the variation of energy with eddy size in isotropic turbulence. They are the three-dimensional energy spectrum, $E(k)$, the one-dimensional energy spectrum, $F_{11}(k)$, and the second-order structure function, $\langle(\Delta v)^2\rangle(r)$, defined as

$$E(k) = \frac{1}{\pi}\int_0^\infty \langle \boldsymbol{u}\cdot\boldsymbol{u}'\rangle kr\sin(kr)\,\mathrm{d}r, \tag{1.1}$$

$$F_{11}(k) = \frac{1}{\pi}\int_0^\infty \langle u_x u_x'\rangle \cos(kr)\,\mathrm{d}r, \tag{1.2}$$

$$\langle(\Delta v)^2\rangle = \langle(u_x' - u_x)^2\rangle, \tag{1.3}$$

where $\langle \boldsymbol{u}\cdot\boldsymbol{u}'\rangle(r)$ is the two-point velocity correlation measured at points separated by the position vector $\boldsymbol{r}$, $r=|\boldsymbol{r}|$, and $\langle u_x u_x'\rangle$ is the longitudinal correlation function measured at points separated by $r\hat{\boldsymbol{e}}_x$. (Here $\hat{\boldsymbol{e}}_x$ is the unit vector in the streamwise direction and $u_x' - u_x = u_x(\boldsymbol{x}+r\hat{\boldsymbol{e}}_x) - u_x(\boldsymbol{x})$.) However, it is well-known that all three diagnostic tools give imperfect measures of the scale-by-scale energy distribution. For example, consider an artificial field of turbulence composed of a sea of eddies (i.e. blobs of vorticity) of fixed size ℓ_e. For simplicity we shall take the vortex blobs to have a Gaussian velocity distribution,

$$\boldsymbol{u} = \Omega r \exp\left[-2r^2/\ell_e^2\right]\hat{\boldsymbol{e}}_\theta,$$

though the results would be little changed if we had chosen a different profile. (Here $\hat{\boldsymbol{e}}_\theta$ is the unit vector in the azimuthal direction.) If these eddies are randomly located and orientated then we find (Davidson 2004)

$$E(k) = \frac{\langle \boldsymbol{u}^2\rangle \ell_e}{24\sqrt{\pi}}(k\ell_e)^4 \exp[-(k\ell_e)^2/4]. \tag{1.4}$$

Evidently, eddies of a given size contribute to all wavenumbers in $E(k)$, their contribution not being restricted to wavenumbers of order $k\sim 1/\ell_e$. Fortunately, however, (1.4) is sharply peaked around $k\sim\pi/\ell_e$, and so this is a deficiency of $E(k)$ which is frequently overlooked. However, the shortcomings of $F_{11}(k)$ and $\langle(\Delta v)^2\rangle$ are not so readily dismissed. For example, it may be shown that (see, for example, Monin & Yaglom 1975)

$$E(k) = k^3\frac{\mathrm{d}}{\mathrm{d}k}\left[\frac{1}{k}\frac{\mathrm{d}F_{11}}{\mathrm{d}k}\right], \tag{1.5}$$

$$F_{11}(k) = \frac{1}{2}\int_k^\infty [1-(k/k^*)^2]\frac{E(k^*)}{k^*}\,\mathrm{d}k^*, \tag{1.6}$$

and so $F_{11}(k)$ represents the weighted sum of $E(k^*)$, integrated from $k^*=k$ to $k^*=\infty$. Thus $F_{11}(k)$ systematically and artificially shifts energy to small k, with $F_{11}(k)$ peaked at $k=0$. For example, for a random sea of Gaussian eddies of fixed size ℓ_e we find, from (1.4) and (1.5),

$$F_{11}(k) = \frac{\langle \boldsymbol{u}^2\rangle \ell_e}{6\sqrt{\pi}}\exp[-(k\ell_e)^2/4]. \tag{1.7}$$

Evidently, in real turbulence, $F_{11}(k)$ provides a flawed measure of the distribution of energy across the different eddy sizes.

The situation is no better with $\langle(\Delta v)^2\rangle$, where it is readily confirmed that, to a good approximation, (Davidson 2004)

$$\frac{3}{4}\langle(\Delta v)^2\rangle(r) \approx \int_{\pi/r}^\infty E(k)\,\mathrm{d}k + (r/\pi)^2\int_0^{\pi/r} k^2E(k)\,\mathrm{d}k. \tag{1.8}$$

In other words, $\frac{3}{4}\langle(\Delta v)^2\rangle$ represents the energy held below scale r, plus $(r/\pi)^2$ times the enstrophy held above scale r. (See § 3, for a detailed discussion of this.) Thus $\langle(\Delta v)^2\rangle$ mixes information about energy and enstrophy, and information about scales smaller and larger than r. So the usual interpretation of $\langle(\Delta v)^2\rangle$, as the cumulative energy held below scale r (Townsend 1976; Landau & Lifshitz 1986) is, at best, a crude approximation. More generally, we see that $\langle(\Delta v)^2\rangle(r)$ is a very leaky filter, admitting information from all scales.

Of course, theoreticians, as well as those involved in numerical simulations, usually work with $E(k)$ or $\langle(\Delta v)^2\rangle$, while experimentalists are necessarily restricted to $F_{11}(k)$ and $\langle(\Delta v)^2\rangle$, or similar one-dimensional quantities. In the limit of Reynolds number $Re \to \infty$, the differences between the various diagnostics is often unimportant in the inertial range as a power law in $E(k)$ gives rise to the same power-law exponent in F_{11}, and a corresponding power law in $\langle(\Delta v)^2\rangle$. For example, the five-thirds law, $E = \alpha\epsilon^{2/3}k^{-5/3}$, corresponds to $F_{11} = \alpha_{11}\epsilon^{2/3}k^{-5/3}$ and $\langle(\Delta v)^2\rangle = \beta\epsilon^{2/3}r^{2/3}$, where $\alpha = 0.761\beta = 55\alpha_{11}/9$. However, at the finite values of Re encountered in numerical simulations and experiments, a power law in $E(k)$ need not correspond to clear power laws in $F_{11}(k)$ or $\langle(\Delta v)^2\rangle$. So, in practice, one must be careful which diagnostic is used. In boundary layer turbulence, for example, it has been shown that $\langle(\Delta v)^2\rangle$ is significantly superior to $F_{11}(k)$ in identifying the range of eddies whose energy scales on the shear velocity (Davidson, Krogstad & Nickels 2006).

In this paper we investigate the limitations of $F_{11}(k)$ and $\langle(\Delta v)^2\rangle$ in detecting inertial-range energy distributions at finite Re. We also look at the limitations of higher-order structure functions, such as $\langle(\Delta v)^4\rangle$. We start with a somewhat idealized model problem, designed to expose the strengths and weaknesses of $E(k)$, $F_{11}(k)$ and $\langle(\Delta v)^2\rangle$ as scale-by-scale measures of energy. We then examine experimental data taken from grid turbulence, comparing the predictions of the model with the data. The comparison is striking.

Our central finding is that, in the inertial range, $\langle(\Delta v)^2\rangle$ takes the form of a mixed power law of the form

$$\langle(\Delta v)^2\rangle = a_1 + a_2 r^2 + a_3 r^{2/3}, \tag{1.9}$$

where $a_2 r^2$ tracks the scale-by-scale variations in enstrophy while $a_3 r^{2/3}$ follows the variation in energy. The 'pollution' of the $r^{2/3}$ law by $a_2 r^2$ is clearly evident in the experimental data.

2. Deficiencies of the second-order structure function

2.1. *An idealized model problem*

In this section we examine a somewhat artificial model problem, designed to expose the weaknesses in $F_{11}(k)$ and $\langle(\Delta v)^2\rangle$ which arise at finite Re. Consider an artificial field of isotropic turbulence composed of a random sea of vortex blobs, which we take to be Gaussian eddies, $\boldsymbol{u} = \Omega r \exp[-2\boldsymbol{x}^2/s^2]\ \hat{\boldsymbol{e}}_\theta$ in (r, θ, z) coordinates. Let the eddies be randomly but uniformly distributed in space, randomly orientated, and have variable energy and size, s. Also, let $\hat{E}(s)$ be the energy density of the turbulence, in the sense that $\hat{E}(s)\mathrm{d}s$ gives the average kinetic energy held in the size range $s \to s + \mathrm{d}s$, and

$$\frac{1}{2}\langle \boldsymbol{u}^2\rangle = \int_0^\infty \hat{E}(s)\,\mathrm{d}s. \tag{2.1}$$

Then it may be shown that (see Davidson 2004)

$$E(k) = \int_0^\infty \frac{\hat{E}(s)s}{12\sqrt{\pi}}(ks)^4 \exp[-(ks)^2/4]\,\mathrm{d}s, \tag{2.2}$$

$$F_{11}(k) = \int_0^\infty \frac{\hat{E}(s)s}{3\sqrt{\pi}} \exp[-(ks)^2/4]\,\mathrm{d}s, \tag{2.3}$$

$$\tfrac{3}{4}\langle(\Delta v)^2\rangle = \int_0^\infty \hat{E}(s)[1 - \exp(-r^2/s^2)]\,\mathrm{d}s. \tag{2.4}$$

Now we are interested in the consequences for E, F_{11} and $\langle(\Delta v)^2\rangle$ of truncating the range of eddy sizes. Suppose, therefore, that the range of eddy sizes is restricted to $\ell < s < L$, with a low L/ℓ corresponding to a small value of Re, and a large L/ℓ to a high value of Re. Moreover, suppose that the kinetic energy held in each decade of scale varies as the power law s^n, i.e.

$$s\hat{E}(s) = \begin{cases} \kappa s^n & \ell < s < L \\ 0, & s < \ell,\ s > L. \end{cases}$$

Then (2.2)–(2.4) are readily integrated to give

$$I_1(k) = E(k)/E^\infty(k) = \frac{1}{\Gamma(a)} \int_{(k\ell/2)^2}^{(kL/2)^2} t^{a-1}\mathrm{e}^{-t}\,\mathrm{d}t, \quad a = \tfrac{1}{2}(n+5), \tag{2.5}$$

$$I_2(k) = F_{11}(k)/F_{11}^\infty(k) = \frac{1}{\Gamma(b)} \int_{(k\ell/2)^2}^{(kL/2)^2} t^{b-1}\mathrm{e}^{-t}\mathrm{d}t, \quad b = \tfrac{1}{2}(n+1), \tag{2.6}$$

$$\frac{\frac{3}{4}\langle(\Delta v)^2\rangle}{\langle \boldsymbol{u}^2\rangle/2} = \frac{nr^n}{L^n - \ell^n} \int_{\ell/r}^{L/r} t^{n-1}[1 - \exp(-1/t^2)]\,\mathrm{d}t. \tag{2.7}$$

where Γ is the gamma function. Here $E^\infty(k)$ and $F_{11}^\infty(k)$ are the functional forms of E and F_{11} in the limit of $L/\ell \to \infty$ with $\ell \ll k^{-1} \ll L$:

$$E^\infty(k) = \frac{2^{n+2}\kappa\Gamma(a)}{3\sqrt{\pi}} k^{-(n+1)}, \tag{2.8}$$

$$F_{11}^\infty(k) = \frac{2^n\kappa\Gamma(b)}{3\sqrt{\pi}} k^{-(n+1)}. \tag{2.9}$$

Since E^∞ and F_{11}^∞ are merely power laws in k, we may regard I_1 and I_2 as so-called compensated forms of E and F_{11}, with $I_1 = I_2 = 1$ for $L/\ell \to \infty$. In the remainder of this section we shall take $n = 2/3$, corresponding to Kolmogorov's 1941 law. In such a case, $E^\infty \sim F_{11}^\infty \sim k^{-5/3}$.

There now arises the issue of how we might relate the size range, $\gamma = L/\ell$, to the Reynolds number in an experiment, such as grid turbulence. Let L be the eddy size at the top of the inertial range, ℓ the eddy size at the bottom of the inertial range, and η the Kolmgorov scale, $(\nu^3/\epsilon)^{1/4}$. Then we expect

$$\epsilon = Au^3/L, \quad \ell = a\eta, \tag{2.10}$$

where ϵ is the rate of dissipation of turbulent kinetic energy, A and a are dimensionless coefficients, $u = \sqrt{\langle u_x^2\rangle}$, ν is the viscosity, and we have assumed that the integral scale of the turbulence is of order L. We expect the coefficients A and a to be of order unity, with a universal but A non-universal, i.e. different for different grid geometries. In terms of the Taylor microscale, λ, we have

$$\lambda^2 = \frac{15\nu u^2}{\epsilon} = \frac{15\nu u^2}{Au^3/L}, \tag{2.11}$$

and combining (2.10) and (2.11) allows us to express γ in terms of the two Reynolds numbers $Re = uL/\nu$ and $R_\lambda = u\lambda/\nu$. After a little algebra we find

$$\gamma = L/\ell = \left(A^{1/4}/a\right) Re^{3/4} = \left(\frac{A}{15^{3/4}a}\right) R_\lambda^{3/2}. \tag{2.12}$$

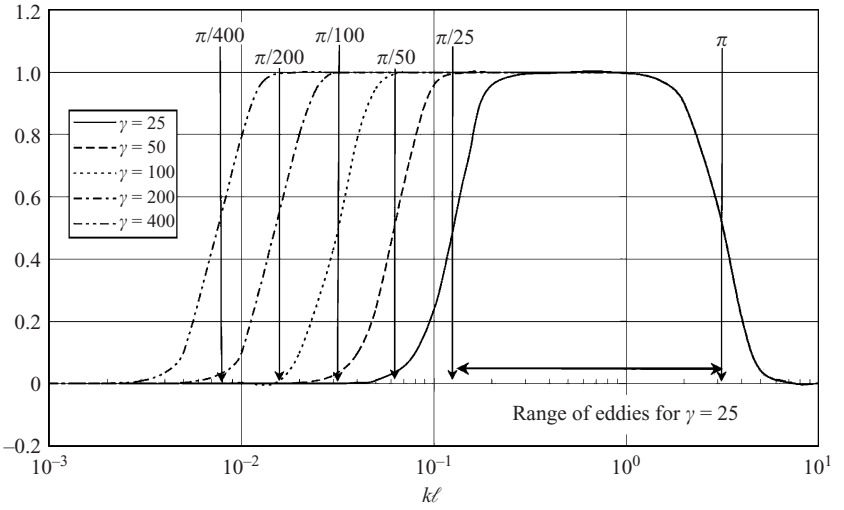

FIGURE 1. Compensated spectra $I_1 \sim k^{5/3}E(k)$ as a function of $k\ell$.

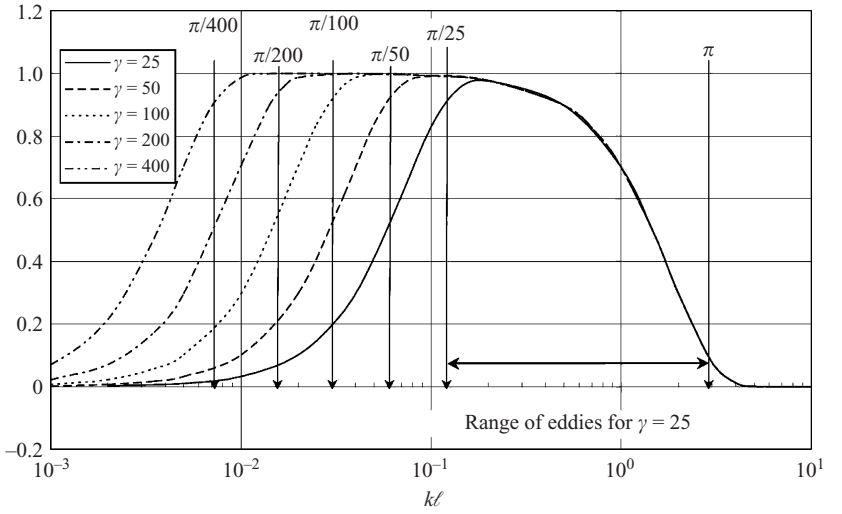

FIGURE 2. Compensated spectra $I_2 \sim k^{5/3}F_{11}(k)$ as a function of $k\ell$.

We shall see in §4 that grid turbulence experiments suggest that $A/a \approx 0.34 \rightarrow 0.45$, depending on the type of grid used. Taking a mean value of $A/a = 0.4$ we have $\gamma \approx 0.0525 R_\lambda^{3/2}$.

Figures 1 and 2 show the three- and one-dimensional compensated energy spectra, $I_1 \sim k^{5/3}E(k)$ and $I_2 \sim k^{5/3}F_{11}(k)$, respectively, as a function of $k\ell$ for $\gamma = 25$, 50, 100, 200 and 400. The vertical lines at π/γ and π indicate the range of eddies present in each case. It is evident that, in this model problem, $E(k)$ displays a clear $k^{-5/3}$ law (corresponding to $I_1 = 1$) for $\gamma \geqslant 50$. The one-dimensional spectrum does less well, systematically and artificially displacing energy to low wavenumbers, as expected. Nevertheless, F_{11} shows evidence of a $k^{-5/3}$ law for $\gamma \geqslant 200$ (i.e. $R_\lambda \geqslant 240$).

Figure 3 shows $\langle(\Delta v)^2\rangle$, normalized by $2u^2$, as a function of r/ℓ for $\gamma = 50$, 200, 400 and 800, the arrows at $r/\ell = 1$ and $r/\ell = \gamma$ indicating the range of eddies in each

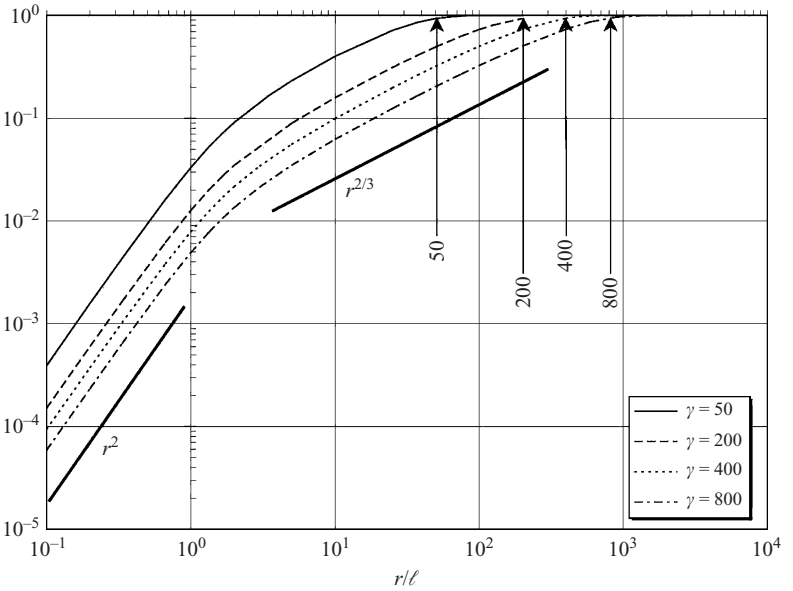

FIGURE 3. Normalized structure function, $\langle(\Delta v)^2\rangle/2u^2$, as a function of r/ℓ; $\gamma =$ 50, 200, 400 and 800.

case. There is no clear $r^{2/3}$ law at $\gamma = 50$ and we do not obtain a decade of $r^{2/3}$ until γ reaches ~ 400 ($R_\lambda \approx 390$). Notice also the $\langle(\Delta v)^2\rangle \sim r^2$ region to the left of $r/\ell = 1$. Clearly, in this model problem, $\langle(\Delta v)^2\rangle$ is an inferior diagnostic tool.

It is an interesting historical footnote that Kolmogorov's 1941 two-thirds law was inspired, in part, by the atmospheric boundary data of Gödecke (1935). Certainly these data show a reasonable $r^{2/3}$ power law. The Reynolds number in Gödecke's measurements was $Re \sim 2 \times 10^4$, corresponding to $\gamma \sim 400$ in our model problem, which is around the minimum value for γ required for a convincing $r^{2/3}$ law.

2.2. *The mixing of information about energy and enstrophy; mixed power laws*

We have already suggested that this failure in $\langle(\Delta v)^2\rangle$ arises from the fact that the second-order structure function mixes information about energy and enstrophy in accordance with (1.8). We may confirm this as follows. The energy spectrum does a reasonable job of tracking the energy distribution for $\gamma \geqslant 50$, so let us approximate $E(k)$ by $E(k) = \kappa k^{-5/3}$, $\pi/L \leqslant k \leqslant \pi/\ell$, while $E(k) = 0$ outside this range. Then (1.8) yields

$$\frac{\frac{3}{4}\langle(\Delta v)^2\rangle}{\langle \boldsymbol{u}^2\rangle/2} \approx \frac{1-\gamma^{-4/3}}{2(\gamma^{2/3}-1)}\left(\frac{r}{\ell}\right)^2, \quad r < \ell, \tag{2.13}$$

$$\frac{\frac{3}{4}\langle(\Delta v)^2\rangle}{\langle \boldsymbol{u}^2\rangle/2} \approx \frac{3(r/\ell)^{2/3} - 2 - \gamma^{-4/3}(r/\ell)^2}{2(\gamma^{2/3}-1)}, \quad \ell < r < L, \tag{2.14}$$

$$\frac{\frac{3}{4}\langle(\Delta v)^2\rangle}{\langle \boldsymbol{u}^2\rangle/2} \approx 1, \quad r > L, \tag{2.15}$$

which is compared with the exact distribution of $\langle(\Delta v)^2\rangle$ in figure 4 for $\gamma = 50$. Evidently, system (2.13)–(2.15) is a good approximation to (2.7), and it has the advantage over the exact distribution in that it makes explicit the reason for the

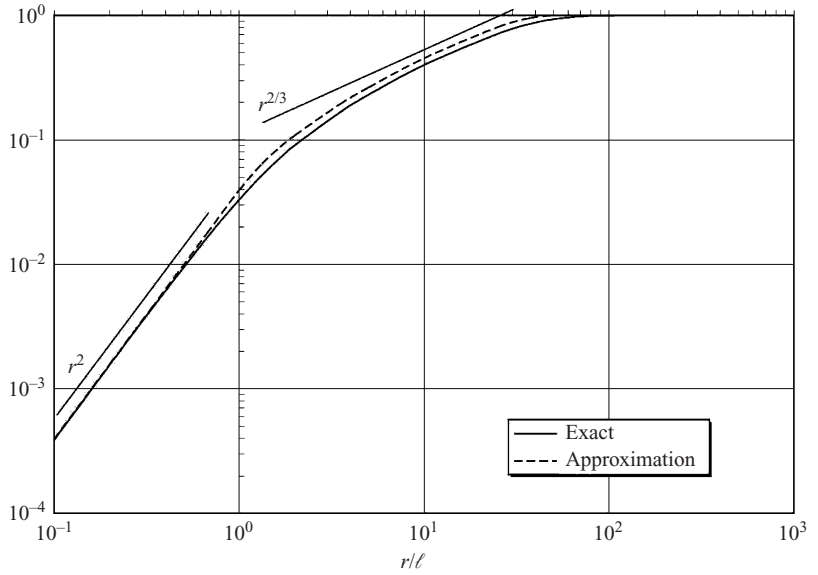

FIGURE 4. Comparison of $\langle(\Delta v)^2\rangle/2u^2$ with approximation (2.13)–(2.15) for $\gamma = 50$.

failure of $\langle(\Delta v)^2\rangle$. Equation (2.13) shows that, for $r < \ell$, the structure function has nothing to do with energy but, rather, reflects the total enstrophy of the population of eddies. Conversely, for $r > L$, the structure function has nothing to do with enstrophy, but rather measures the total energy. For $\ell < r < L$, there is a mixture of two power laws, $r^{2/3}$ and r^2, with the former tracking the energy of the eddies and the latter tracking the enstrophy in accordance with (1.8). Thus the failure of $\langle(\Delta v)^2\rangle$ to display a clear $r^{2/3}$ law at modest values of γ arises from the contamination of the structure function by enstrophy, as measured by the second integral on the right of (1.8). Note that, as $\gamma \to \infty$ in (2.14), we recover the two-thirds law for $r \ll L$. However, rewriting (2.14) as

$$\frac{\frac{3}{4}\langle(\Delta v)^2\rangle}{\langle \boldsymbol{u}^2\rangle/2} \approx \frac{3(r/L)^{2/3} - (r/L)^2 - 2\gamma^{-2/3}}{2 - 2\gamma^{-2/3}} \tag{2.16}$$

it is clear that we still have mixed power-law behaviour when r/L is of order unity, even in the limit of $\gamma \to \infty$.

We note in passing that, if we had adopted the conventional interpretation of $\langle(\Delta v)^2\rangle$, as the cumulative energy held below scale r (Townsend 1976; Landau & Lifshitz 1986), i.e. $\frac{3}{4}\langle(\Delta v)^2\rangle(r) \approx \int_{\pi/r}^{\infty} E(k)\,\mathrm{d}k$, then (2.14) simplifies to

$$\frac{\frac{3}{4}\langle(\Delta v)^2\rangle}{\langle \boldsymbol{u}^2\rangle/2} \approx \frac{(r/\ell)^{2/3} - 1}{\gamma^{2/3} - 1}, \quad \ell < r < L, \tag{2.17}$$

and the mixed power law disappears. We shall compare both (2.14) and (2.17) with experimental data in §4. While (2.14) is an excellent fit to the data, (2.17) is not.

Finally we note that Batchelor (1951) suggested that $\langle(\Delta v)^2\rangle$ can be expressed as a sort of hybrid power law of the form $\langle(\Delta v)^2\rangle \sim \epsilon^{2/3} r^{2/3} g(r/\eta)$, where $g(x) = x^{4/3}(1 + \delta x^2)^{-2/3}$ and δ is a constant. However, we emphasize that this is simply an interpolation between the two expressions $\langle(\Delta v)^2\rangle = \langle(\partial u_x/\partial x)^2\rangle r^2$ and $\langle(\Delta v)^2\rangle = \beta\epsilon^{2/3} r^{2/3}$ which hold for $r \ll \eta$ and $r \gg \eta$ respectively in the limit $Re \to \infty$.

3. The implications for other even-order structure functions

We now consider the implications of our analysis for higher-order structure functions. Our starting point is to return to (1.8). From a mathematical point of view this expression originates from the exact relationship between $\langle(\Delta v)^2\rangle$ and $E(k)$:

$$\tfrac{3}{4}\langle(\Delta v)^2\rangle = \int_0^\infty E(k)H(kr)\,\mathrm{d}k, \tag{3.1}$$

where

$$H(\chi) = 1 + 3\chi^{-2}\cos\chi - 3\chi^{-3}\sin\chi. \tag{3.2}$$

Now a reasonable approximation to $H(\chi)$ is

$$\hat{H}(\chi) = \begin{cases} (\chi/\pi)^2, & \chi < \pi \\ 1, & \chi > \pi, \end{cases} \tag{3.3}$$

and substituting $\hat{H}(\chi)$ for $H(\chi)$ in (3.1) yields (1.8). From a physical perspective, however, we can rationalise (1.8) as follows. Let us consider turbulence to be composed of an ensemble of eddies of size s_1, plus an ensemble of size s_2 etc., from η up to the integral scale L. Each ensemble is taken to be isotropic in its own right. If $s_i \ll r$ then the correlation length of these eddies will be much smaller than r and the corresponding contribution to $\langle(\Delta v)^2\rangle$ is simply $\langle(\Delta v)^2\rangle_{s_i} = 2\langle u_x^2\rangle_{s_i} = (2/3)\langle \boldsymbol{u}^2\rangle_{s_i}$, where the subscript s_i indicates the contribution to $\langle(\Delta v)^2\rangle$ or $\langle u_x^2\rangle$ from the eddies of size s_i. Conversely, if $s_i \gg r$, then the contribution to $\langle(\Delta v)^2\rangle$ from these relatively large eddies is $\langle(\Delta v)^2\rangle_{s_i} = \langle(\partial u_x/\partial x)^2\rangle_{s_i} r^2 = \frac{1}{15}\langle\boldsymbol{\omega}^2\rangle_{s_i} r^2$. In summary then,

$$\tfrac{3}{4}\langle(\Delta v)^2\rangle = \tfrac{1}{2}\langle\boldsymbol{u}^2\rangle_s, \quad s \ll r, \tag{3.4}$$

$$\tfrac{3}{4}\langle(\Delta v)^2\rangle = \tfrac{1}{2}\langle\boldsymbol{\omega}^2\rangle_s \frac{r^2}{10}, \quad s \gg r. \tag{3.5}$$

If we now classify all eddies as belonging to one or other group, which is clearly unsatisfactory when $s \sim r$, then we have

$$\tfrac{3}{4}\langle(\Delta v)^2\rangle(r) \approx \tfrac{1}{2}[\langle\boldsymbol{u}^2\rangle^S + (r^2/10)\langle\boldsymbol{\omega}^2\rangle^L] \tag{3.6}$$

where the superscripts S and L indicate the contribution to the energy and enstrophy which comes from eddies smaller or larger than r, respectively. In terms of $E(k)$ this is written

$$\tfrac{3}{4}\langle(\Delta v)^2\rangle(r) \approx \int_{\pi/r}^\infty E(k)\,\mathrm{d}k + (r^2/10)\int_0^{\pi/r} k^2 E(k)\,\mathrm{d}k. \tag{3.7}$$

We have arrived back at (1.8), but with π^2 replaced by 10.

Let us now apply the same reasoning to the higher-order structure functions. As before, we take the contribution to Δv from eddies smaller than r as $\sqrt{2}\,(u_x)_{s_i}$ while the contribution from eddies larger than r is $r\,(\partial u_x/\partial x)_{s_i}$. Then we have

$$\Delta v \approx \sum_{s_i<r} \sqrt{2}\,(u_x)_{s_i} + \sum_{s_i>r} r(\partial u_x/\partial x)_{s_i}. \tag{3.8}$$

If we now assume that the contributions from scales larger than r are decorrelated from those smaller than r, and that single-point velocity statistics are Gaussian, we obtain

$$\langle(\Delta v)^2\rangle \approx 2\langle u_x^2\rangle^S + r^2\langle(\partial u_x/\partial x)^2\rangle^L, \tag{3.9}$$

which is the same as (3.6), and

$$\langle(\Delta v)^3\rangle \approx r^3\langle(\partial u_x/\partial x)^3\rangle^L, \tag{3.10}$$

$$\langle(\Delta v)^4\rangle \approx 12\left[\left\langle u_x^2\right\rangle^S\right]^2 + 12r^2\left\langle u_x^2\right\rangle^S\langle(\partial u_x/\partial x)^2\rangle^L + r^4\langle(\partial u_x/\partial x)^4\rangle^L, \tag{3.11}$$

etc.

Now (3.8) is clearly an over simplification. Nevertheless (3.11) suggests that, just like $\langle(\Delta v)^2\rangle$, the fourth-order structure function is a very leaky filter, mixing information about large and small scales, and about energy and velocity gradients. We note in passing that (3.10) suggests that $\langle(\Delta v)^3\rangle$ does not share this difficiency, though it is emphasized that (3.10) does not apply to $\langle|\Delta v|^3\rangle$.

Now one of the consequences of this smearing of information in $\langle(\Delta v)^2\rangle$ is highlighted by (2.14): we do not obtain a single power law for $\langle(\Delta v)^2\rangle$, but rather a mixture of two, one tracking the scale-by-scale variation in energy and the other tracking the enstrophy. It is this combination of power laws which masks the two-thirds law at modest values of γ. Estimate (3.11) suggests that there is a corresponding problem for $\langle(\Delta v)^4\rangle$, and indeed for all even-power structure functions. This, in turn, suggests that, for finite γ, an attempt to fit a single power law to $\langle(\Delta v)^p\rangle$ throughout the inertial range will result in a systematic deviation from the Kolmogorov 1941 scaling (K41) $\langle(\Delta v)^p\rangle \sim r^{p/3}$. Of course, this particular departure from K41 has nothing at all to do with intermittency, but simply reflects the leaky nature of structure functions.

We shall show data that suggest that higher-order structure functions do indeed follow mixed power laws.

4. Comparison with experimental data

The model problem described in § 2.1 is much too idealized to be considered representative of real turbulence. Nevertheless, the central notion embedded in (1.8), that $\langle(\Delta v)^2\rangle$ mixes information about enstrophy and energy, is robust. We might expect, therefore, that real turbulence exhibits a behaviour not unlike (2.13)–(2.15), with a mixed power law in the inertial range.

In order to test this idea, a set of experiments was performed in grid-generated turbulence. The measurements were performed in the large wind tunnel at The Norwegian University of Science and Technology, which has a test section 2 m high by 2.7 m wide, with a length of 11 m. Two grids were used. One was a conventional grid made of square bars of 46×46 mm cross-section forming a square mesh with a mesh size of 240 mm. In order to make the turbulent Reynolds number as high as possible, a second grid was created from the first by blocking every alternate mesh. This increased the grid solidity from 34.7 % to 67.3 %. The measurements were performed at $x = 9.3$ m from the grid, corresponding to $x/M = 37.2$. With the conventional grid the tunnel speed was restricted to $U = 18.5\,\mathrm{m\,s^{-1}}$. Owing to the significant blocking caused by the second grid, this dropped to about $U = 12\,\mathrm{m\,s^{-1}}$ when the modified grid was installed. Measurements were made for $180 \leqslant R_\lambda \leqslant 320$ using the conventional grid and $290 \leqslant R_\lambda \leqslant 660$ with the modified grid.

The measurements were taken using 2.5 μm single hot wires with a ratio of wire length, w, to Kolmogorov length scale, η, ranging from $w/\eta = 0.9$ to 2.9. From initial measurements of the power density spectra at high sampling rates, the point where electronic noise started to affect the dissipation spectrum was determined. The signal

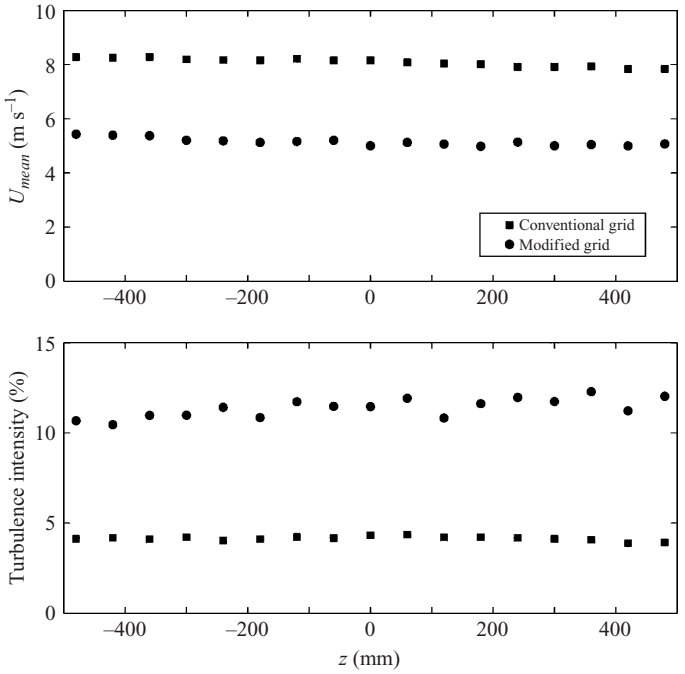

FIGURE 5. Mean velocity and turbulence intensity distributions across the flow at $x/M = 37.2$.

was then low-pass filtered at this frequency and the sampling frequency was set slightly higher than twice this frequency.

The severe blocking of the second grid may raise concerns about the flow homogenity. To check if the non-uniformity caused by the blocked grid had died out at the measurement station, a number of spanwise traverses were made across four meshes for both grids at $x/M = 37.2$. Figure 5 shows an example of such a traverse which demonstrates that the uniformity of both the mean velocity and the turbulence intensity was about the same for both grids. Even though the turbulence intensity does not show any spanwise inhomogenities, it is known that high grid solidity may cause a flapping motion in the flow due to the interaction of the jets formed by the grid. This will appear as isolated peaks of increased energy in the low-frequency part of the spectrum. The shedding frequency is expected to depend linearly on the flow velocity and should therefore be found in the power spectra at increasing frequency as the velocity is increased. Figure 6 shows the low-frequency part of the spectra for a range of mean velocities from about $U = 2.5$ to $10\,\mathrm{m\,s^{-1}}$. Assuming $f_{flapping} \sim U/M$ we would expect the range of frequencies to be roughly from 10 to 40 Hz. There are no indications of a velocity-dependent energy peak in the plotted energy distributions. (The full-range power density spectra are shown in figure 7.)

For each test condition the signal was sampled in six batches of about 4×10^6 samples to ensure that the full range of the energy spectrum was resolved. Figure 7 shows a selection of the measured Kolmogorov-scaled streamwise one-dimensional spectra as function of Reynolds number for both grids. The collapse is seen to be quite good and for the highest R_λ the inertial subrange covers about two decades of k. The corresponding second-order structure functions are shown in figure 8.

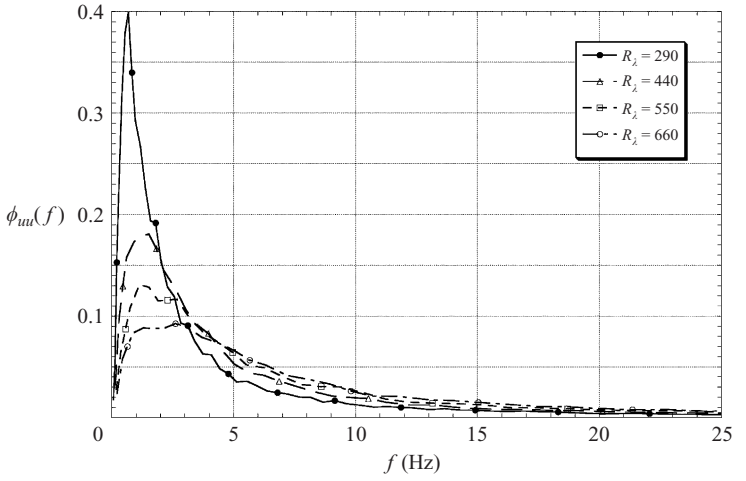

FIGURE 6. Low-frequency part of the power density spectra.

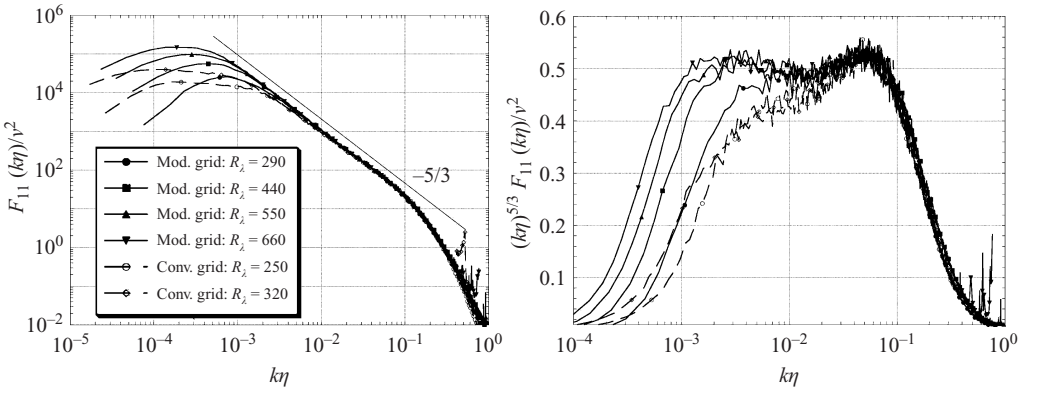

FIGURE 7. (*a*) Power density spectra. (*b*) Compensated power density spectra.

The dissipation rate, ϵ, used to estimate the Kolmogorov scales, was obtained using three independent methods. Assuming small-scale isotropy, ϵ was computed from

$$\epsilon_1 = \frac{15\nu}{U^2}\langle(\partial u/\partial t)^2\rangle.$$

The second estimate was obtained by integrating the dissipation spectrum,

$$\epsilon_2 = 15\nu \int_0^\infty k_1^2 F_{11}(k_1)\,\mathrm{d}k_1.$$

Finally, ϵ was estimated from the inertial subrange using

$$F_{11}(k_1) = C_1\epsilon_3^{2/3}k_1^{-5/3}.$$

The three estimates agreed for all cases to within $\pm 10\%$; most of the time even better.

The issue now arises whether or not the measured structure functions exhibit a mixed power-law behaviour of the form suggested by (1.8) and (2.13)–(2.15). In short, does $\langle(\Delta v)^2\rangle$ take the form

$$\langle(\Delta v)^2\rangle \sim a_1 + a_2 r^2 + a_3 r^{2/3} \tag{4.1}$$

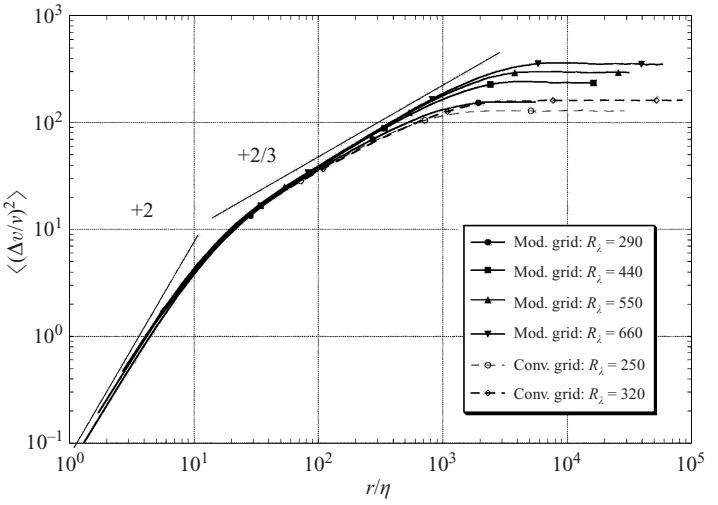

FIGURE 8. Measured $\langle(\Delta v)^2\rangle$ scaled with Kolmogorov variables.

in the inertial subrange? Despite the naivity of the model problem outlined in § 2.1, it seems natural to compare the data directly with predictions (2.13)–(2.15), which have the advantage of containing only one free parameter, as we shall now show.

The right-hand sides of (2.13)–(2.15) contain the unknowns γ and ℓ. However, these are not independent as (2.13) must be compatible with

$$\frac{\frac{3}{4}\langle(\Delta v)^2\rangle}{\langle \boldsymbol{u}^2\rangle/2} \rightarrow \frac{r^2}{2\lambda^2} \tag{4.2}$$

for $r \rightarrow 0$, and this demands that

$$\ell^2 = \frac{1-\gamma^{-4/3}}{\gamma^{2/3}-1}\lambda^2 \,. \tag{4.3}$$

Moreover we have seen that

$$\gamma = cR_\lambda^{3/2}/15^{3/4}, \quad c = A/a, \tag{4.4}$$

for some dimensionless coefficient, c, which should be of the order of, though somewhat less than, unity. Thus, if c is specified, then (4.4) fixes γ and (4.3) determines ℓ. In comparing the data with (2.13)–(2.15), therefore, we need only settle on the value of c.

Now A, and hence c, is non-universal and may vary from one geometry to another. Indeed energy decay measurements for the two grids show that the ratio of A for the conventional and modified grid is $A_{con}/A_{mod} = 1.33$, and so we require c for the conventional mesh to be 33 % higher than that for the modified grid. For the present purposes, we have chosen $c = 0.337$ for the modified grid and $c = 0.448$ for the conventional mesh.

Figures 9(a) to 9(d) show the comparison of (2.13)–(2.15) with the measured structure functions for the modified grid ($R_\lambda = 290$, 440, 550 and 660), while figures 10(a) and 10(b) show the comparison for the conventional grid ($R_\lambda = 250$ and 320). Given the naivity of the model, the comparison is striking for both sets of data, confirming the mixed power-law behaviour of $\langle(\Delta v)^2\rangle$ in the inertial range. In order to emphasize the point, figures 9 and 10 also show the pure power-law estimate

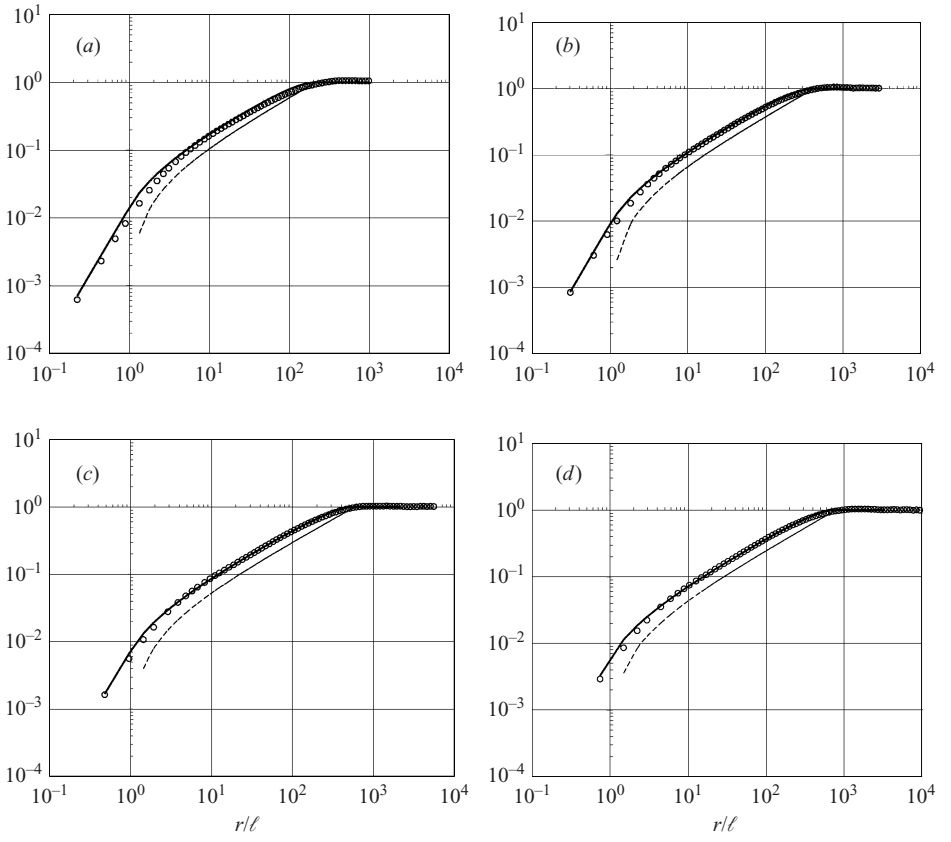

FIGURE 9. Comparison between the measured $\langle(\Delta v)^2\rangle/2$ and equations (2.13)–(2.15) for the modified grid. Symbols are measurements and curves the theoretical predictions. The dashed line represents the pure power law, equation (2.17). (*a*) $R_\lambda = 290$, (*b*) $R_\lambda = 440$, (*c*) $R_\lambda = 550$, (*d*) $R_\lambda = 660$.

of $\langle(\Delta v)^2\rangle$, (2.17), based on the traditional, but incorrect, interpretation of $\langle(\Delta v)^2\rangle$ in which the enstrophy contribution is neglected, i.e.

$$\tfrac{3}{4}\langle(\Delta v)^2\rangle = \int_{\pi/r}^{\infty} E(k)\,\mathrm{d}k. \tag{4.5}$$

The fit is much less satisfactory, as we would expect.

Note that, for large γ, (2.16) and (2.17) simplify to

$$\frac{\frac{3}{4}\langle(\Delta v)^2\rangle}{\langle \boldsymbol{u}^2\rangle/2} = \tfrac{3}{2}(r/L)^{2/3} - \tfrac{1}{2}(r/L)^2, \quad \ell \ll r < L, \tag{4.6}$$

$$\frac{\frac{3}{4}\langle(\Delta v)^2\rangle}{\langle \boldsymbol{u}^2\rangle/2} = (r/L)^{2/3}, \quad \ell \ll r < L, \tag{4.7}$$

which is independent of γ, and hence of c and R_λ. Thus the main differences between the combined power-law form of $\langle(\Delta v)^2\rangle$, which is an excellent fit to the data, and the spurious single power-law estimate of $\langle(\Delta v)^2\rangle$, which comes from (4.5), are independent of the choice of the coefficient c. The single power-law estimate of $\langle(\Delta v)^2\rangle$ is clearly inferior.

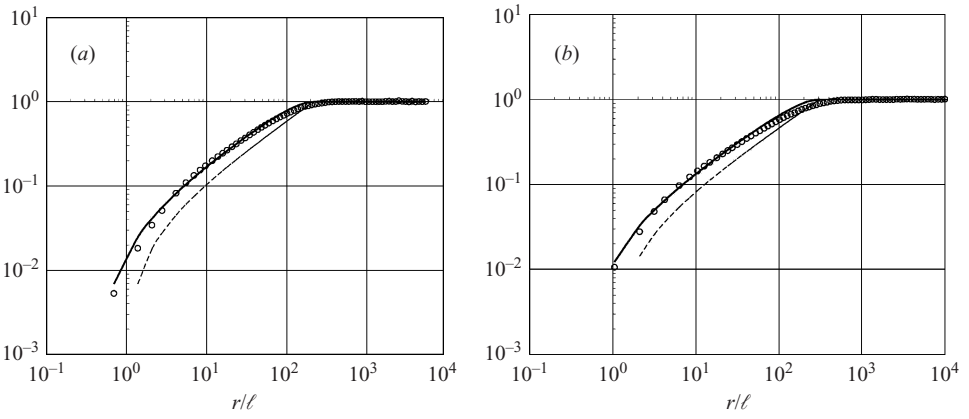

FIGURE 10. Comparison between $\langle(\Delta v)^2\rangle/2$ and equations (2.13)–(2.15) for the conventional grid. Symbols are measurements. The dashed line represents the pure power law, equation (2.17). (*a*) $R_\lambda = 250$, (*b*) $R_\lambda = 320$.

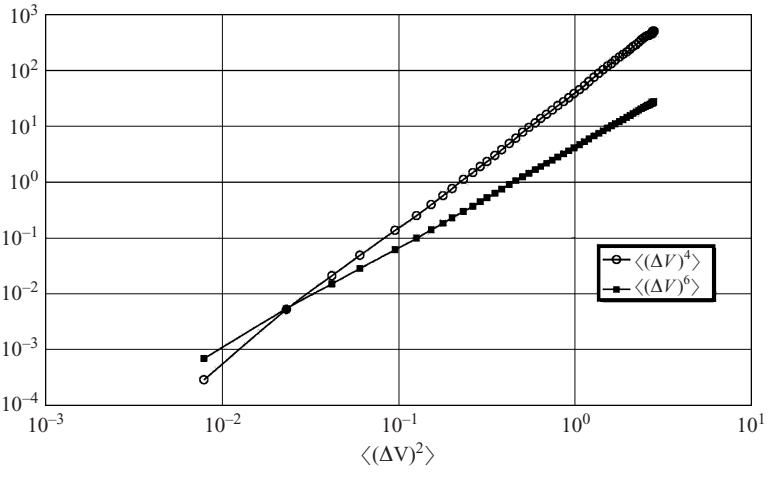

FIGURE 11. $\langle(\Delta v)^4\rangle$ and $\langle(\Delta v)^6\rangle$ plotted against $\langle(\Delta v)^2\rangle$ for $R_\lambda = 660$.

Finally we consider fourth-order structure functions. This time we cannot compare the data directly with our simple model, since (3.11) contains the unknown quantity $\langle(\partial u_x/\partial x)^4\rangle^L$. However, it is an empirical observation, which has yet to be explained, that even-order structure functions are related by power laws of the type

$$\langle(\Delta v)^p\rangle \sim \langle(\Delta v)^2\rangle^{\alpha_p}, \quad \alpha_p = \text{constant},$$

throughout the inertial and dissipation ranges. This is the basis of the so-called extended-self-similarity of the equilibrium range and is illustrated in figure 11. This figure shows $\langle(\Delta v)^4\rangle$ and $\langle(\Delta v)^6\rangle$ for the modified grid at $R_\lambda = 660$, plotted against $\langle(\Delta v)^2\rangle$. Given that $\langle(\Delta v)^2\rangle$ exhibits mixed-power-law behaviour in the inertial range, it seems inevitable that all higher-order structure functions of even-order must do the same.

5. A footnote: the deficiencies of one-dimensional spectra

So far we have focused on the deficiencies of $\langle(\Delta v)^2\rangle$ as an inertial-range diagnostic. However, in § 1 and § 2 we saw that F_{11} is also a flawed diagnostic, and indeed this has already been emphasized by Davidson *et al.* (2006) in the context of large-scale eddies in boundary layers. We close with a brief discussion of the problems associated with inertial-range measurements of F_{11}.

The model problem of § 2.1 is somewhat artificial, designed mainly to expose the deficiencies of $\langle(\Delta v)^2\rangle$. Let us now move to something closer to real turbulence and consider a simple model of the equilibrium range. As before, our interest lies in exposing the limitations of the various diagnostic tools. However, whereas we focused on the deficiencies of the second-order structure function in § 2–§ 4, we now focus on the weaknesses of F_{11}.

According to Kolmogorov's 1941 theory the skewness of (Δv),

$$S = \langle(\Delta v)^3\rangle / \langle(\Delta v)^2\rangle^{3/2}, \tag{5.1}$$

is constant across the inertial subrange. While subsequent refined models, incorporating intermittency, suggest that S may vary with r, this predicted variation lies within the scatter of the experimental data. Moreover, it is an empirical observation that the skewness in the dissipation range is not very different to that in the inertial range, varying from $S \sim -0.3$ at the bottom of the inertial range to $S \sim -0.4$ at the Kolmogorov scale. Thus a very simple, but plausible, model of the equilibrium range is Obukhov's constant-skewness model. This takes the equilibrium-range version of the Kármán–Howarth equation, where $\partial\langle(\Delta v)^2\rangle/\partial t$ is neglected,

$$6\nu\frac{\partial}{\partial r}\langle(\Delta v)^2\rangle - S\langle(\Delta v)^2\rangle^{3/2} = \tfrac{4}{5}\epsilon r, \tag{5.2}$$

and adds to it the closure hypothesis that S is constant for all r and equal to its equilibrium-range value, $S = -\frac{4}{5}\beta^{-3/2}$. Here β is Kolmogorov's constant in the two-thirds law: $\langle(\Delta v)^2\rangle = \beta\epsilon^{2/3}r^{2/3}$. Introducing the scaled variables

$$y = \frac{\langle(\Delta v)^2\rangle}{\beta(15\beta)^{1/2}v^2}, \quad x = \frac{r}{(15\beta)^{3/4}\eta}, \tag{5.3}$$

where η and v are the Kolmogorov length and velocity scales, the resulting equation for $\langle(\Delta v)^2\rangle$ is simply

$$\tfrac{1}{2}y'(x) + y^{3/2} = x, \tag{5.4}$$

which is readily integrated. The predictions of this simple closure model are surprisingly good, as indicated by Figure 6.19 in Davidson (2004), which compares the integration of (5.4) with the direct numerical simulations of Fukayama *et al.* (2001) at $R_\lambda = 460$. The corresponding form of the compensated energy spectrum is also shown in Davidson (2004) in Figure 6.47. It clearly exhibits an overshoot, or bump, at the junction of the inertial and dissipation ranges. This is the well-known bottle-neck effect, which is a purely viscous phenomenon. The overshoot in $E(k)$ is around 40 % in the constant-skewness model and a bottle-neck of similar (though slightly smaller) intensity is evident in the direct numerical simulations of Kaneda *et al.* (2003) at $R_\lambda = 1200$. (See also the experiments of Davidson & Pearson 2005.)

Now we know that F_{11} artificially and systematically shifts energy to low k, so it is of interest to look at the corresponding form of F_{11}. It is readily confirmed that the bottle-neck is largely suppressed in F_{11}. This may be seen by looking at figure 7(*b*) or at high-Re data of Saddoughi & Veeravalli (1994), where there is virtually no

bottle-neck in F_{11}. Alternatively, one can calculate F_{11} from $\langle(\Delta v)^2\rangle$ in the constant-skewness model. Again, it is readily confirmed that the bottle-neck is largely suppressed, with the excess energy transferred to lower k. (See, for example, Strobel 2005.) The net effect is that F_{11} gives the impression of an extended inertial range.

6. Conclusions

We have shown that the second-order structure function is a poor filter, in the sense that it mixes information from large and small scales and information about energy and enstrophy. One consequence of this is that, in the inertial range, it takes the form of a mixed power law of the form

$$\langle(\Delta v)^2\rangle \sim a_1 + a_2 r^2 + a_3 r^{2/3}$$

with r^2 tracking the enstrophy of the eddies and $r^{2/3}$ tracking the energy. This is the reason why Kolmogorov's two-thirds law is harder to realize than the equivalent spectral five-thirds law. We have illustrated this with a simple model problem which gives a surprisingly good fit to measurements made in grid turbulence.

We emphasize that it is not just the second-order structure function which suffers from this problem, all even-order structure functions mix information from large and small scales, and this calls into question the physical interpretation of measured anomalous scaling exponents for higher-order structure functions.

The authors would like to thank Tim Nickels for useful discussions during the preparation of this work and the referees for valuable inputs that have improved the quality of the paper.

REFERENCES

Batchelor, G. K. 1951 Pressure fluctuations in isotropic turbulence. *Proc. Camb. Phil. Soc.* **47**, 359–374.

Davidson, P. A. 2004 *Turbulence, An introduction for Scientists and Engineers*. Oxford University Press.

Davidson, P. A., Krogstad, P.-Å. & Nickels, T. B. 2006 A refined interpretation of the logarithmic structure function law in wall layer turbulence. *Phys. Fluids* **18**, 065112.

Davidson, P. A. & Pearson, B. 2005 Identifying turbulent energy distributions in real, rather than Fourier, space. *Phys. Rev. Let.* **95**, 214501.

Fukayama D., Nakano, T., Bershadskii, A. & Gotoh, T. 2001 Local properties of extended self-similarity in three-dimensional turbulence. *Phys. Rev.* E **64**, 016304.

Gödecke, K. 1935 Measurements of atmospheric turbulence. *Ann. Hydrogr.* **10**, 400–410.

Kaneda, Y., Ishihara, T., Yokokawa, M., Itakura, K. & Uno, A. 2003 Energy dissipation rate and energy spectrum in high resolution DNS. *Phys. Fluids* **15**, L21.

Landau, L. D. & Lifshitz, L. M. 1986 *Fluid Mechanics*, 2nd edn., Pergamon.

Monin, A. S. & Yaglom, A. M. 1975 *Statistical Fluid Mechanics II* MIT Press.

Saddoughi, S. G. & Veeravalli, S. V. 1994 Measuring turbulent energy distributions in real space. *J. Fluid Mech.* **268**, 333–372.

Strobel, L. 2005 The mystery of the turbulent bottleneck. *Cambridge Univ. Engng. Dept. Technical Report*.

Townsend, A. A. 1976 *The Structure of Turbulent Shear Flows*, 2nd edn. Cambridge University Press.